ISSN 0020-1685, Inorganic Materials, 2016, Vol. 52, No. 8, pp. 802–810. © Pleiades Publishing, Ltd., 2016.
Original Russian Text © I.V. Mazilin, L.Kh. Baldaev, D.V. Drobot, E.Yu. Marchukov, N.G. Zaitsev, 2016, published in Neorganicheskie Materialy, 2016, Vol. 52, No. 8, pp. 865–873.

Phase Composition and Thermal Conductivity of Zirconia-Based Thermal Barrier Coatings

I. V. Mazilin[a], L. Kh. Baldaev[a], D. V. Drobot[b], E. Yu. Marchukov[c], and N. G. Zaitsev[a]

[a] *OOO Technological Systems for Protective Coatings, Simferopol'skoe sh. 19, Shcherbinka, Moscow oblast, 142172 Russia*
[b] *Lomonosov State University of Fine Chemical Technologies, Moscow Technological University, pr. Vernadskogo 86, Moscow, 119571 Russia*
[c] *Lyul'ka Experimental Design Bureau, Ufa Engine Industrial Association Public Joint Stock Company, ul. Kasatkina 13, Moscow, 129301 Russia*
e-mail: imazilin@gmail.com

Received May 27, 2015; in final form, February 19, 2016

Abstract—Atmospheric plasma spraying of powder materials has been used to produce thermal barrier coatings (TBCs) based on ZrO_2 stabilized with 7 wt % Y_2O_3, including coatings doped with neodymium and samarium oxides, for state-of-the-art and next-generation high-temperature gas turbine engines. Doping with neodymium and samarium oxides has been shown to reduce the thermal conductivity of the TBCs by 10–20%. At the same time, changes in the phase composition, crystal structure parameters, and microstructure of the TBCs during heat treatment at the service temperature lead to an increase in the thermal conductivity of all the coatings by 50–70%.

Keywords: thermal barrier coating, zirconia, rare-earth oxides, thermal conductivity
DOI: 10.1134/S0020168516080124

INTRODUCTION

Thermal barrier coatings (TBCs) are widely used to protect blades and other parts of the hot section of gas turbine engines (GTEs) from high temperatures, erosive wear, and corrosion [1]. Materials based on zirconia stabilized with 7 wt % yttria (ZrO_2–$7Y_2O_3$) have been used as the main ceramic layer of TBCs for more than 35 years now. Coatings based on this oxide possess a unique combination of properties: low thermal conductivity, stably high thermal expansion coefficient, and mechanical properties outstanding among ceramic materials [2–4].

One of the most topical areas in the development of ZrO_2–$7Y_2O_3$-based TBCs at present is the ability to reduce their thermal conductivity and improve their durability by doping. According to data in the literature, rare-earth oxides are best suited for this purpose: the properties of TBCs have been improved by completely or partially replacing yttria by gadolinia, dysprosia, ytterbia, scandia, and other rare-earth oxides [5–10]. Nevertheless, systematic data on the influence of the chemical and phase compositions, microstructure, and the time at the service temperature on the thermophysical properties of TBCs are essentially missing in the literature.

The purpose of this work is to assess the influence of each of these parameters on the thermal diffusivity and thermal conductivity of zirconia-based TBCs. We have proposed a new TBC composition, containing yttrium, neodymium, and samarium oxides as stabilizers and possessing reduced thermal conductivity.

In nonconductive nonmagnetic solids, heat transport follows two main mechanisms: a phonon mechanism, which is the result of crystal lattice vibrations, and a photon mechanism, which is due to thermal radiation. The relative contributions of these mechanisms to the total thermal conductivity of the material are temperature-dependent. In the service temperature range of GTEs (20–1200°C), the phonon mechanism prevails. It can be represented by the equation [11]

$$k(T) = C_V(T)l_p(T)v, \quad (1)$$

where C_V (J/(g K)) is the isochoric specific heat, l_p (m) is the phonon mean free path, and v (m/s) is the phonon velocity.

To reduce the thermal conductivity, the three components should be reduced, but the phonon mean free path makes the largest contribution. The existence of a particular value of l_p is due to phonon scattering by lattice defects (vacancies, interstitial atoms, interstitial and substitutional impurity atoms, dislocations, and grain boundaries) and other phonons.

Table 1. Characteristics of the powders and coatings

Composition of the powder, wt %	Tapped density, g/cm^3	Particle size composition (size fractions), %			Coating designations	Spray parameters		Coating thickness, μm	Coating porosity, vol %
		>60 μm	60–40 μm	40–20 μm		*P*, kW	*L*, mm		
ZrO_2–$7Y_2O_3$	1.1	24.3	34.9	40.6	I-1	46	90	1011	10
					I-3	43	60	745	11
ZrO_2–$7Y_2O_3$	1.9	33.3	37.7	28.8	II-1	46	90	898	9
					II-2	39	60	1087	11
					II-5	46	60	821	12
ZrO_2–$7Y_2O_3$–$5Nd_2O_3$–$5Sm_2O_3$	2.2	47.2	28.1	24.4	III-10	49	60	916	12
					III-12	49	90	825	20

Consider the mechanism of phonon scattering by dopant atoms. In this case, l_p is given by [9]

$$\frac{1}{l_p} = \frac{a^3}{4\pi v^4}\omega^4 c\left(\frac{\Delta M}{M}\right)^2, \quad (2)$$

where a is the atomic volume, v is the wave velocity, ω is the phonon frequency, C is the concentration per atom, M is the atomic mass of the host material, and ΔM is the atomic mass of the dopant.

It should be noted that l_p is proportional to the square of the ratio of the atomic masses of the host and dopant. Since zirconium and yttrium differ little in atomic mass, phonon scattering by yttrium atoms is insignificant. The 1000°C thermal conductivity of sintered samples with the composition ZrO_2–$7Y_2O_3$ is at a level of 2.3 W/(m K) [2].

The thermal conductivity of a TBC depends on its microstructure, which is determined by the coating procedure and process conditions. The 1000°C thermal conductivity of ZrO_2–$7Y_2O_3$-based TBCs produced by atmospheric plasma spraying (APS) is 1.8–2.0 W/(m K) [8], because they contain pores and have a layered microstructure. Coatings with the same composition grown by electron beam physical vapor deposition (EB-PVD) have a columnar structure and a thermal conductivity near 2.0 W/(m K) at 1316°C [10]. As shown by Zhu and Miller [10], codoping of zirconia with two oxides, one of a light rare earth (La–Gd) and the other of a heavy rare earth (Dy–Yb), leads to a 40% decrease in the thermal conductivity of coatings produced by electron beam physical vapor deposition.

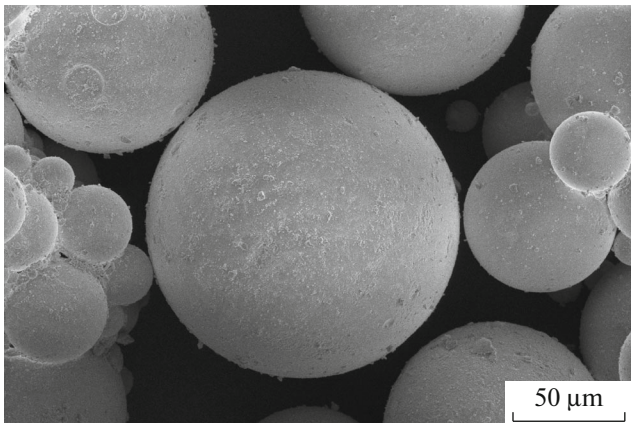

Fig. 1. Morphology of powder I (SEM).

EXPERIMENTAL

Coating procedure. Coating samples for this investigation were prepared by atmospheric plasma spraying using an HVP system (Technological Systems for Protective Coatings, Russia) equipped with an F4 plasma torch. The plasma gas used was a mixture of argon and hydrogen.

As starting materials for spraying, we used various powders (Table 1). The powders were prepared by the reverse precipitation method. The working solution was prepared using zirconium and yttrium chlorides (powder I) and acetates (powders II and III). In the preparation of powder III, the doping elements were introduced into the solution as neodymium and samarium nitrates. The working solution was added with stirring to an excess of aqueous ammonia. The resultant gel was washed, filtered, and dried. The semifinished product thus obtained was calcined in a muffle furnace. According to scanning electron microscopy (SEM) data, most of the particles in powders I–III were spherical in shape (Fig. 1) and ranged in size from 10 to 90 μm. The particle size compositions (sieve analysis) and tapped density of powders I–III are indicated in Table 1. It is worth noting that the loose bulk density of powder I is considerably lower than that of powders II and III. Given that the powders are similar in chemical and particle size compositions, this suggests that powder I has closed porosity.

The powders for the preparation of coatings were fed into a plasma jet in radial direction at the tip of a plasma gun nozzle. For this purpose, we used a PF 2/2

Table 2. X-ray diffraction data for the powders and coatings

Sample	Phase	Weight percent	R_{wp}	a, Å	c, Å	Crystallite size, nm	Lattice strain ε, %	ρ_x, g/cm^3
Powders								
I	t'-ZrO_2	100	10.7	3.6247 (4)	5.1705 (8)	21.8 (3)	0.47 (3)	5.9534 (17)
II	t'-ZrO_2	100	10.2	3.6199 (2)	5.1750 (3)	21.7 (3)	0.90 (3)	5.9642 (70)
III	t-ZrO_2	100	–	3.636 (1)	5.117 (9)	–	–	–
As-sprayed coatings								
I-1	t'-ZrO_2	98.6 (2)	12.4	3.6158 (2)	5.1699 (3)	251 (8)	0.40 (1)	5.9835 (6)
I-3	t'-ZrO_2	98.5 (2)	13.0	3.6161 (2)	5.1701 (4)	271 (9)	0.42 (1)	5.9821 (8)
II-1	t'-ZrO_2	97.8 (4)	13.6	3.6140 (1)	5.1667 (2)	254 (7)	0.43 (1)	5.9931 (3)
II-2	t'-ZrO_2	94.0 (9)	10.7	3.6137 (1)	5.1665 (2)	216 (8)	0.42 (1)	5.9944 (3)
II-5	t'-ZrO_2	98.5 (2)	13.0	3.6148 (1)	5.1680 (2)	234 (8)	0.46 (1)	5.9889 (6)
Coatings heat-treated at the service temperature								
I-3T	t'-ZrO_2	64.4 (1)	12.9	3.6134 (1)	5.1686 (2)	>1000	0.29 (1)	5.9930 (4)
	t-ZrO_2	35.6 (15)		3.6120 (3)	5.1649 (6)	153 (27)	0.75 (3)	6.0731 (12)
II-2T	t'-ZrO_2	70.4 (2)	13.4	3.6132 (1)	5.1689 (2)	>1000	0.31 (1)	5.9933 (5)
	t-ZrO_2	29.6 (19)		3.6107 (6)	5.1662 (12)	87 (19)	0.80 (8)	6.0759 (26)
II-5T	t'-ZrO_2	68.2 (1)	12.8	3.6131 (1)	5.1685 (2)	>1000	0.31 (1)	5.9942 (4)
	t-ZrO_2	31.8 (13)		3.6115 (3)	5.1646 (7)	123 (20)	0.83 (4)	6.0752 (14)
III-10T	t'-ZrO_2	72.7 (1)	12.8	3.6283 (3)	5.1624 (3)	>1000	0.32 (1)	5.9511 (9)
	t-ZrO_2	27.3 (13)		3.6174 (21)	5.1448 (35)	161 (75)	1.21 (7)	6.0786 (83)
III-12T	t'-ZrO_2	54.1 (1)	12.6	3.6285 (2)	5.1635 (2)	>1000	0.32 (1)	5.9490 (8)
	t-ZrO_2	45.9 (10)		3.6289 (11)	5.1441 (35)	194 (63)	1.34 (4)	6.0409 (56)

powder feeder (GTV, Germany). The carrier gas used was argon. The plasma spraying process parameters were adjusted for each powder by assessing the microstructure, porosity, amount of cracking, and density of other defects in 12 coatings produced at varied plasma power and spraying standoff distance. At the spray parameters thus chosen (Table 1), we obtained thick coatings (700–1200 μm). To confirm the reliability of the data obtained, thermophysical measurements and X-ray diffraction characterization were carried out for at least two identical samples.

The coating samples were heat-treated in an SNOL 2.5-15 muffle furnace at a temperature of 1250°C for 24 h.

Coating composition and structure determination. X-ray diffraction patterns of the powders and coatings were collected on a D8 Advance diffractometer (Bruker, Germany). The intensity data collection parameters were as follows: CuK_{α_1} radiation (λ = 1.5406 Å), angular range 2θ = 10°–100°, scan step Δ2θ = 0.05°, and scan rate 2°/min. In qualitative phase analysis of the samples, we used ICDD PDF-2 data. The quantitative phase composition and structural parameters of the samples were determined by the Rietveld method. The agreement factors R_{wp} are listed in Table 2.

The microstructure of the coatings was examined using polished cross-sections which were prepared in several steps. The samples were cut on a Brilliant 220 precision cut-off machine (ATM, Germany) and then potted in epoxy. The specimens were ground and polished on a Saphir 550 pneumatic machine (ATM, Germany). To prepare surfaces for microstructural analysis, we used a grinding wheel, waterproof P600 sandpaper, cloth wheels, and diamond slurries (9, 3, and 1 μm steps). To examine the microstructure of the coatings and evaluate their thickness, we used an Axiovet 40 MAT optical microscope (Zeiss, Germany). A Versa 3D scanning electron microscope (FEI, USA) equipped with a microanalysis system was used to examine the morphology of the powders, determine the porosity and microstructural characteristics of the coatings, and perform microanalysis of inclusions. Images were obtained using secondary-electron and backscattered-electron detectors.

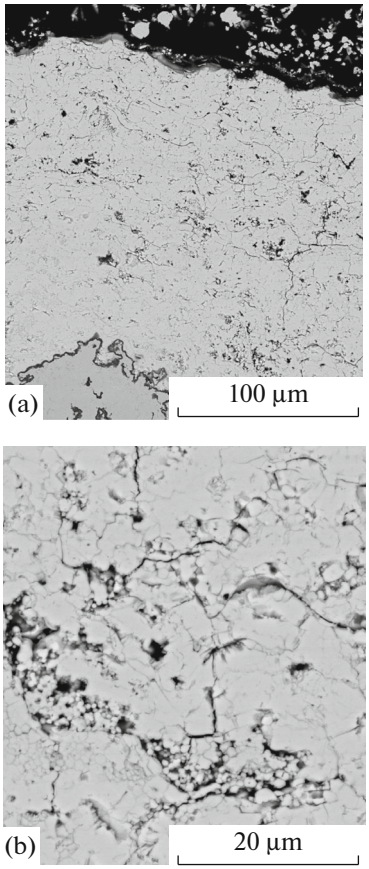

Fig. 2. Microstructure of coatings (a) I-3 and (b) II-2 (SEM).

Thermal conductivity determination. Thermal diffusivity was measured with an LFA 457 apparatus (Netzsch, Germany) by the laser flash method in conformity with the ASTM E1461 Standard, using free-standing coating samples in the form of rectangular parallelepipeds. Before measurements, a colloidal graphite layer was produced on the samples to ensure identical emissivity values. Thermal diffusivity was measured in an argon atmosphere at temperatures from 20 to 1000°C at 100°C intervals.

Heat capacity was determined indirectly, by comparing the temperature rise signal from the sample (during heat front propagation) to that from a reference sample (Pyroceram 9606).

The density of the samples was determined by hydrostatic weighing. The results were compared to the density calculated from the X-ray density of the coating and its porosity evaluated by electron microscopy.

EXPERIMENTAL RESULTS

Microstructure of the coatings. According to SEM data (Fig. 2a), coatings I–III were 740 to 1090 μm in thickness (Table 1) and contained no microstructural defects (cracks or delaminations). At a larger magnification, the coatings are seen to have a layered microstructure characteristic of plasma spray coatings (Fig. 2b). The density of the coatings had a significant effect on their thermophysical properties, so special attention was paid to reliable density measurements. According to electron microscopy data, coatings I–III were uniform in porosity. The volume fraction of pores in the coatings was evaluated by graphical analysis of electron micrographs (Table 1). The porosity of coatings III slightly exceeds that of coatings I and II, which is due to the fact that powder III contained a larger percentage of coarse particles. Moreover, it had the highest tapped density and required more energy for being heated. The microhardness of the coatings was $HV_{0.2}$ = 5.5–7.0 GPa. Heat treatment at the service temperature did not affect the microstructure of the coatings: their porosity remained unchanged and no cracks or other defects were detected. Their microhardness increased slightly, to $HV_{0.2}$ = 8.0–10.0 GPa.

Phase composition of the coatings. X-ray diffraction characterization showed that, in contrast to the starting powders, the as-sprayed coatings I–III consisted of a mixture of the t'-ZrO_2 and m-ZrO_2 phases. The formation of the monoclinic phase can be accounted for by the specifics of the plasma spraying process, which is characterized by extremely high cooling rates of particles impact on the substrate (>10^6 K/s). In most of the coatings, the content of the monoclinic phase did not exceed 2%, except for sample II-2 (6%), which was probably caused by incomplete melting of the particles in the plasma jet. The unit-cell parameters of the major phase in coatings I–III differed little and were essentially independent of spraying conditions. The unit-cell parameters c and a of the coatings were smaller than those of the starting powders, but the degree of tetragonality (c/a ratio) remained unchanged (~1.011). The crystallite size of the major phase in the coatings was an order of magnitude greater than that in the starting powders, reaching 200–300 nm.

After heat treatment at the service temperature, the samples of coatings IT–IIIT consisted of a mixture of tetragonal zirconia phases, t-ZrO_2 and t'-ZrO_2, which differed in unit-cell parameters. It should be noted that the crystallite size of the major phase considerably exceeded both the crystallite size of the second phase and that of the t'-ZrO_2 phase before heat treatment. No reflections from m-ZrO_2 were detected. The unit-cell parameters of coatings III are distinctive in that they have a low degree of tetragonality (~1.006), which is due to the doping with neodymium and samarium oxides.

Specific heat of the coatings. The experimentally determined specific heats of the coatings exhibit similar behavior, rising with increasing temperature (Fig. 3), and differ by no more than 10%. It should be noted that the specific heat of all coatings II decreases

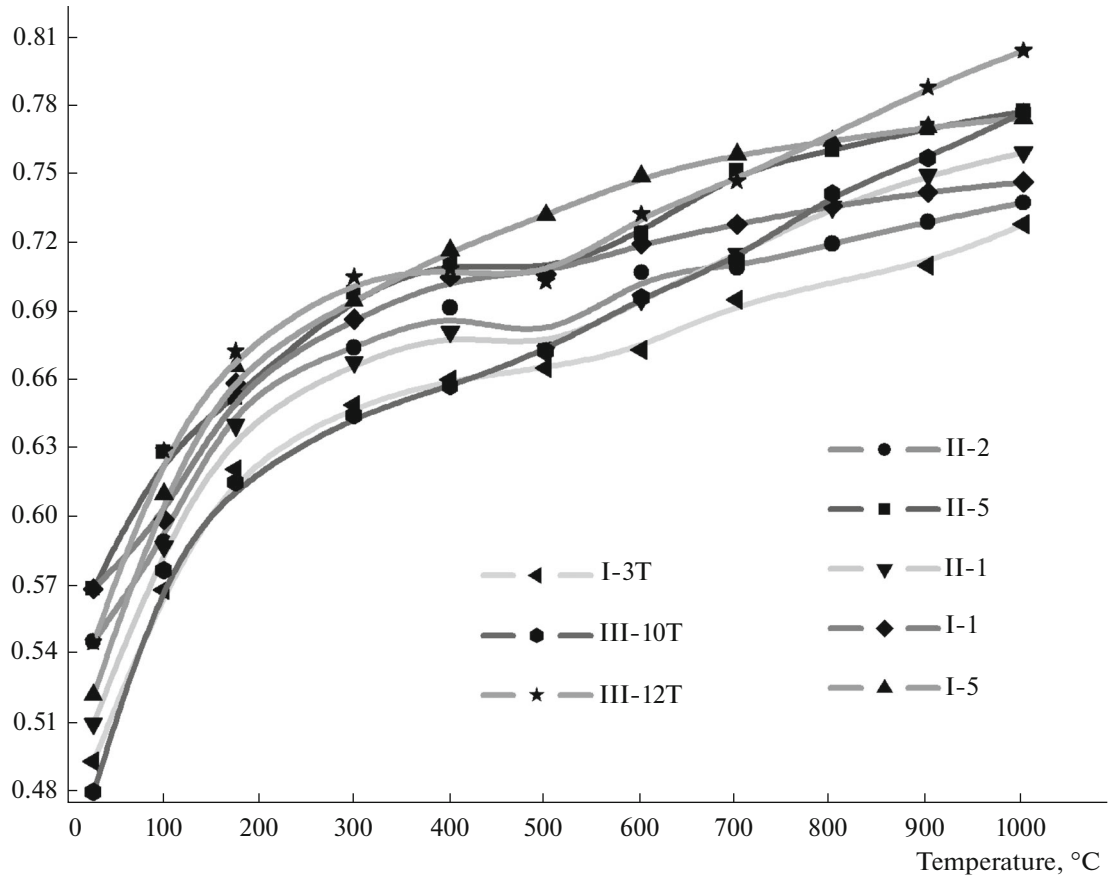

Fig. 3. Specific heat as a function of temperature for the coatings.

slightly near 500°C and continues to rise at higher temperatures.

Thermal diffusivity of the coatings. Using the laser flash method, we obtained temperature dependences of thermal diffusivity for the coatings in the range 20–1000°C (Fig. 4). The thermal diffusivity decreases with increasing temperature, which is characteristic of dielectrics at $T > \Theta_D$ (Debye characteristic temperature), where their thermal diffusivity is determined by the phonon mechanism of heat transport. The data can be represented roughly as $\alpha \sim 1/T$. Coatings II-2 have the lowest thermal diffusivity, which may be associated with the highest m-ZrO_2 content and the smallest crystallite size of the major phase t'-ZrO_2 (Fig. 4a). The thermal diffusivity of the other coatings is 10–15% higher.

Heat treatment at the service temperature increased the thermal diffusivity of all the coatings by 60–80%. The hatched region in Fig. 4b illustrates the spread in the thermal diffusivity of coatings IT and IIT. It should be noted that the thermal diffusivity of coating III-10T, which is comparable in porosity and phase composition to the other coatings, is 15–25% lower because of the doping.

Thermal conductivity of the coatings. Using the measured thermal diffusivity, specific heat, and density of the coating samples and the well-known relation (3) [11], we obtained the temperature dependence of their thermal conductivity:

$$\lambda(T) = \alpha(T)C_V(T)\rho, \quad (3)$$

where α (mm^2/s) is thermal diffusivity, C_V (J/(g K)) is specific heat, and ρ (g/cm^3) is density.

The temperature behavior of the thermal conductivity of the coatings is governed by the temperature dependence of their thermal diffusivity, except in the low-temperature region (<200°C), where the measured specific heat showed large scatter. The slight decrease in the specific heat of some coatings at 500°C influenced their thermal conductivity as well (Fig. 5a).

Heat treatment at the service temperature increased the thermal conductivity of all the coatings by 50–70% (Fig. 5b). At temperatures above 700°C, we observe an increase in the thermal conductivity of coatings IIIT. The reason for this is that, in this temperature range, the specific heat of coatings III, which contain neodymium and samarium oxides, increases more rapidly (Fig. 3) than their thermal diffusivity decreases (Fig. 4b).

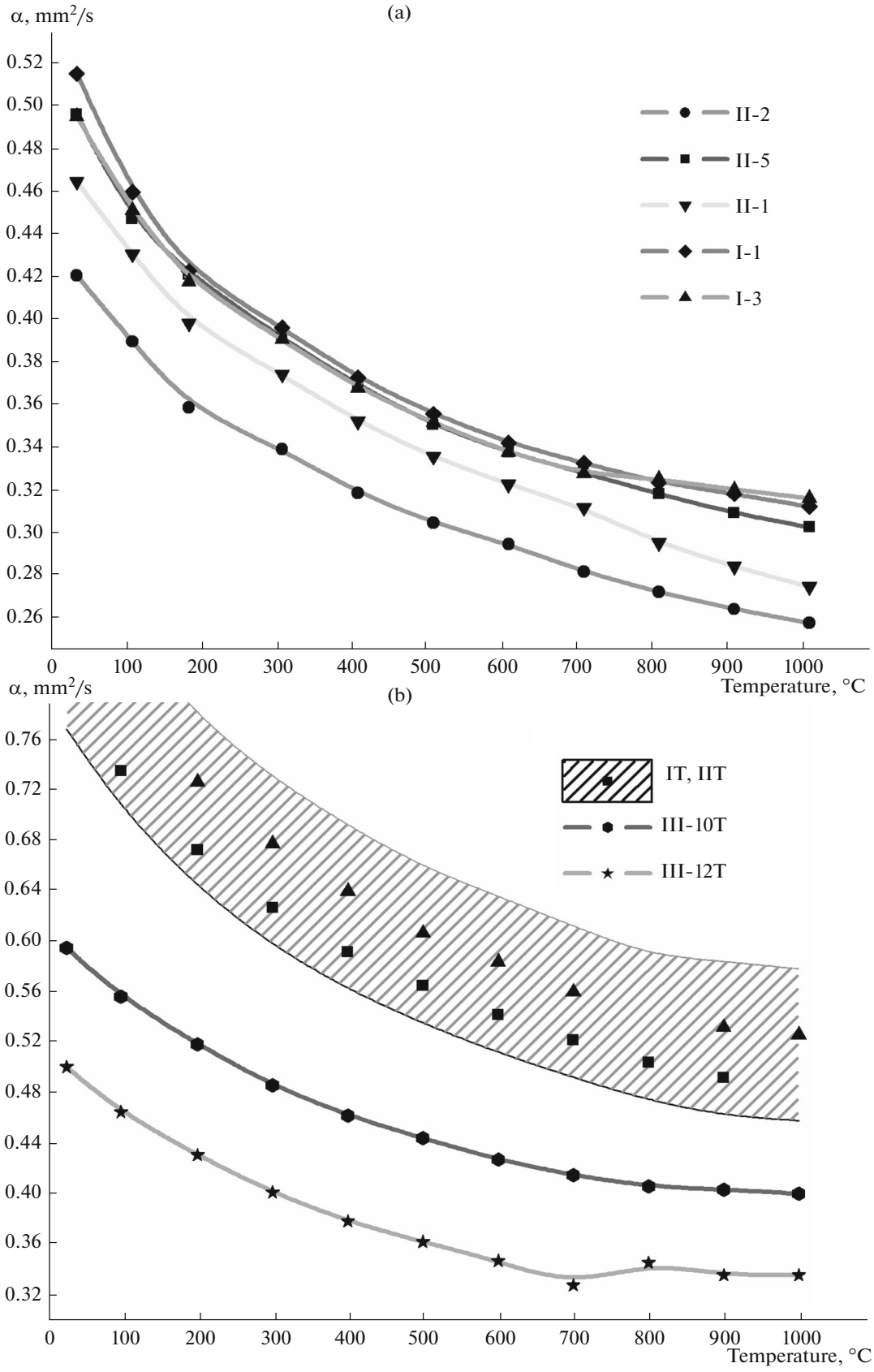

Fig. 4. Thermal diffusivity as a function of temperature for the coatings (a) before and (b) after heat treatment at 1250°C.

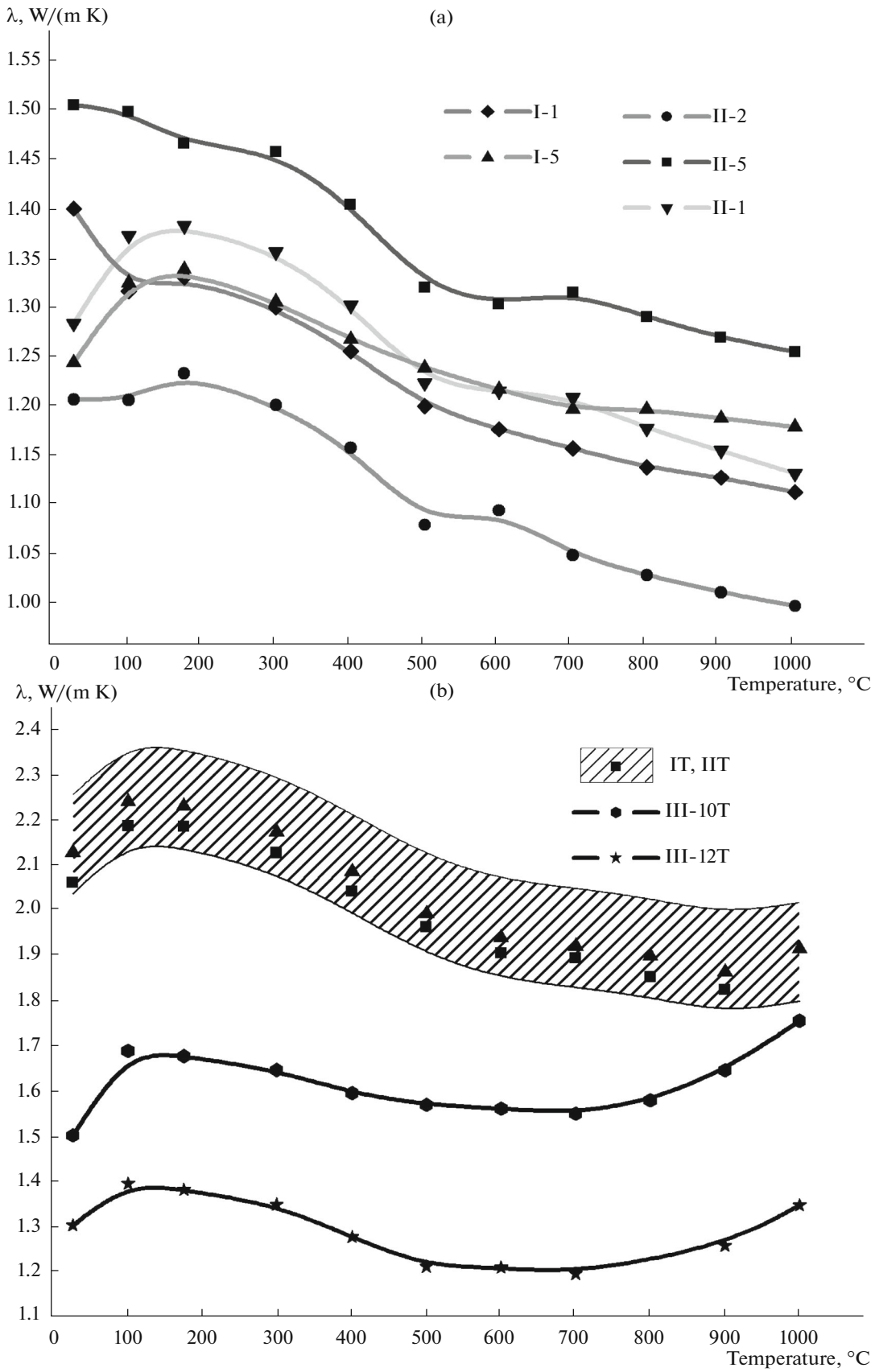

Fig. 5. Thermal conductivity as a function of temperature for the coatings (a) after spraying and (b) after heat treatment at 1250°C.

DISCUSSION

The present experimental data suggest that the thermal conductivity of the thermal barrier coatings is influenced by the following parameters: chemical composition, microstructure, porosity, phase composition, and structural parameters.

Effect of chemical composition. Comparison of the thermal conductivity of coatings III, doped with neodymium and samarium oxides, and coatings I and II, which have a standard chemical composition, demonstrates that producing point defects is an effective approach for obtaining coatings with low thermal conductivity: a decrease by 10–20% was reached at comparable porosities and phase compositions. Codoping with two or more oxides appears to be more effective than doping with the same amount of one oxide. It is also necessary that dopant atoms be heavier and larger than yttrium atoms. In choosing the amount of a dopant, it should be taken into account that the thermal conductivity of coatings is influenced by their specific heat and that their durability is influenced by the degree of tetragonality of the t'-ZrO_2 phase. Doping with 5 wt % neodymium and samarium oxides increases the temperature effect on the specific heat of the coatings, which shows up as an increase in calculated thermal conductivity in the temperature range from 700 to 1000°C.

Effects of phase composition and crystal structure parameters. The phase composition of the coatings remained essentially unchanged in all the steps of the study of their thermophysical properties, with only slight distinctions in the case of the samples of coatings III, due to the doping. The effect of the heat treatment time at the service temperature is much better defined. Clearly, the thermal conductivity of the coatings after heat treatment is considerably higher than that after spraying. This is due to changes in the phase composition and crystal structure parameters of the phases present, as well as to changes in microstructure.

The plasma spray coatings I–III are characterized by the presence of phases that are metastable for the composition and conditions under consideration (m-ZrO_2). Since heat transport in the coatings is predominantly due to crystal lattice vibrations, the presence of such "defects" reduces it. In the course of high-temperature service, the phase composition of such coatings becomes more homogeneous, their crystal structure undergoes ordering, and their crystallite size increases. In combination, these processes lead to an increase in their thermal conductivity.

Effects of the porosity and microstructure of the coatings. The microstructure of the plasma spray coatings contains characteristic defects in the form of microcracks, pores, and interfaces between layers. Their density also influences the thermal conductivity of the coatings, the volume fraction of pores being the main factor.

Clearly, the thermal conductivity of the coatings decreases with increasing porosity. In this study, this is best illustrated by comparison of samples III-10T and III-12T, which have porosities of 12 and 20% and 1000°C thermal conductivities of 1.75 and 1.35 W/(m K), respectively.

The effect of the heat treatment time at the service temperature shows up as "healing" of microstructural defects (interfaces between layers and microcracks). This process also leads to an increase in the thermal conductivity of the coatings. Note, however, that the thermal conductivity of the coatings increases sharply only during the first few hours of service. Subsequently, it varies only slightly because of sintering (decrease in porosity).

CONCLUSIONS

Thermal barrier coatings based on ZrO_2 stabilized with 7 wt % Y_2O_3, including coatings doped with neodymium and samarium oxides, have been produced by a plasma spraying method (APS). Using SEM and X-ray diffraction, we have determined their composition and structure and analyzed the changes observed during the plasma spraying process and heat treatment at the service temperature with respect to the starting materials.

The thermophysical properties of the coatings have been investigated by the laser flash method. Doping with neodymium and samarium oxides has been shown to reduce the thermal conductivity of the TBCs by 10–20%. At the same time, changes in the phase composition, crystal structure parameters, and microstructure of the TBCs during heat treatment at the service temperature lead to an increase in the thermal conductivity of all the coatings by 50–70%.

The present findings confirm that the thermal conductivity of zirconia-based thermal barrier coatings can be reduced by doping with rare-earth oxides and that the use of expensive dysprosium and ytterbium oxides, proposed by Zhu and Miller [10], is unnecessary.

REFERENCES

1. Miller, R.A., Thermal barrier coatings for aircraft engines: history and directions, *J. Therm. Spray Technol.,* 1997, vol. 6, no. 1, pp. 35–42.
2. Levi, C., Emerging materials and processes for thermal barrier systems, *Curr. Opin. Solid State Mater. Sci.,* 2004, vol. 8, pp. 77–91.
3. Cao, X.Q., Vassen, R., and Stoever, D., Ceramic materials for thermal barrier coatings, *J. Eur. Ceram. Soc.,* 2004, vol. 24, no. 1, pp. 1–10.
4. Evans, A.G., Clarke, D.R., and Levi, C.G., The influence of oxides on the performance of advanced gas turbines, *J. Eur. Ceram. Soc.,* 2008, vol. 28, pp. 1405–1419.

5. Cao, X.Q., Application of rare earths in thermal barrier coating materials, *J. Mater. Sci. Technol,* 2007, vol. 23, no. 1, pp. 15–35.

6. Liu, H.S., Li, Q., Li, Y., et al., Microstructure, phase stability and thermal conductivity of plasma sprayed Yb_2O_3, Y_2O_3 co-stabilized ZrO_2 coatings, *Solid State Sci.,* 2011, vol. 13, no. 3, pp. 513–519.

7. Curry, N., Markocsan, N., Ostergren, L., Li, X., and Dorfman, M., Evaluation of the lifetime and thermal conductivity of dysprosia-stabilized thermal barrier coating systems, *J. Therm. Spray Technol.,* 2013, vol. 22, no. 6, pp. 864–872.

8. Gupta, M., Curry, N., Nylen, P., Markocsan, N., and Vassen, R., Design of next generation thermal barrier coatings—experiments and modeling, *Surf. Coat. Technol.,* 2013, vol. 220, pp. 20–26.

9. Nicholls, J.R., Lawson, K.J., Johnstone, A., and Rickerby, D.S., Methods to reduce the thermal conductivity of EB-PVD TBCs, *Surf. Coat. Technol.,* 2002, vols. 151–152, pp. 383–391.

10. Zhu, D. and Miller, R., Development of advanced low conductivity thermal barrier coatings, *Int. J. Appl. Ceram. Technol.,* 2004, vol. 1, no. 1, pp. 86–94.

11. Tritt, T., *Thermal Conductivity: Theory, Properties, and Applications,* New York: Kluwer, 2004.